

Molecular photodissociation enabled by ultrafast plasmon decay

José Torres-Sánchez¹ and Johannes Feist^{1, a)}

*Departamento de Física Teórica de la Materia Condensada and Condensed Matter Physics Center (IFIMAC),
Universidad Autónoma de Madrid, E-28049 Madrid, Spain*

(Dated: 23 March 2022)

We propose a strategy for enabling photodissociation of a normally photostable molecule through coupling to a nanoparticle plasmon. The large possible coupling on the single-molecule level combined with the highly lossy nature of plasmonic modes, with lifetimes on the order of femtoseconds, opens an ultrafast decay channel for the molecule. For plasmon mode frequencies below the vertical photoexcitation energy of the molecule, the difference between excitation and emission energy is converted into vibrational energy on the molecular ground state in a Raman-like process. Under the correct conditions, this energy can be high enough to enable efficient photodissociation on the electronic ground state. We demonstrate the concept using numerical simulations of the Lindblad master equation for the hydrogen molecule in the vicinity of an aluminum nanoparticle, and explore the photodissociation efficiency as a function of various system parameters.

I. INTRODUCTION

Polaritonic chemistry and molecular polaritonics are fields inspired by the possibility to manipulate and control molecular structure and dynamics through strong interactions with confined electromagnetic modes. Interest in these possibilities has increased strongly over the last few years from a range of different and previously independent disciplines. General overviews over the possibilities afforded in such systems can be found in a series of reviews published over the last years^{1–6}. Most initial interest was focused on “macroscopic” settings where a (large) collection of molecules interacts with optical cavity modes (e.g., in Fabry-Perot planar mirror cavities), and in which the so-called strong-coupling regime can be reached relatively easily with organic molecular materials⁷. This regime is reached when the (collective) interaction strength between light and matter excitations becomes larger than the relevant dissipation rates in the system. The excitations of the coupled system then become hybrid light-matter excitations, so-called polaritons, that are split in energy by the so-called Rabi splitting. In particular, the possibility to manipulate (photo)chemical reactions in such settings has been demonstrated experimentally^{8–12} and analyzed theoretically^{13–20}.

While collective light-matter coupling involving a macroscopic number of molecules can be used to modify a variety of molecular properties, its influence at the single-molecule level is limited due to the delocalized nature of polaritons in such settings^{13,19–21}. Much larger and more direct changes at the single-particle level can be achieved by increasing the single-molecule coupling strength, which requires increasing the confinement of the electromagnetic field modes. In order to approach the single-molecule strong coupling limit at room temperature and with the dipole transition strengths available in organic molecules, strongly subwavelength field confinement is required, which in turn requires that the real part of the dielectric permittivity of the “cavity” material becomes negative²². At optical frequencies, this essentially means that the only

currently available setups with significant single-molecule coupling strengths are based on metallic structures supporting plasmonic resonances (i.e., oscillations of the free electrons in the metal). In such systems, strong coupling can be reached with relatively few emitters²³, even down to the single-molecule level^{24,25}. It has also been shown that such setups can be used to modify molecular reactions such as photo-oxidation²⁶. However, plasmonic resonances unavoidably come with large losses due to a significant fraction of their energy being stored in the motion of free electrons in the metal²². The resulting resonance lifetimes are typically on the order of 10 fs, short compared to the time needed for most chemical reactions to take place. Very recently, theoretical efforts have thus started to be directed towards making virtue out of necessity, i.e., towards exploiting the ultrafast loss in plasmonic nanocavities and nanoantennas to achieve desired functionalities^{27–31}.

Along similar lines, in this manuscript we devise a strategy for using ultrafast decay induced by coupling to plasmonic modes to permit photodissociation in molecules that do not normally do so upon photoexcitation. The general idea is to induce ultrafast decay at a specific position on the excited-state potential energy surface (PES) in such a way that the kinetic energy accumulated by the nuclei after photoexcitation at the Franck-Condon point is sufficient to overcome the dissociation barrier on the ground-state electronic surface after photon loss, even when photodissociation is not energetically allowed on the excited-state PES. We demonstrate the concept using the simplest neutral molecule, hydrogen (H_2). It turns out that the potential energy curves for the two lowest electronic states of H_2 exactly fulfill the conditions for which the process we propose takes place efficiently. Additionally, aluminum nanoantennas can provide plasmonic resonances with the required characteristics (energy and decay rate).

II. THEORY

The system we consider, sketched in the inset of Fig. 1, consists of a single hydrogen molecule close to an aluminum nanoparticle. The molecular electronic structure is approximated by the lowest two electronic states within the Born-

^{a)}Electronic mail: johannes.feist@uam.es

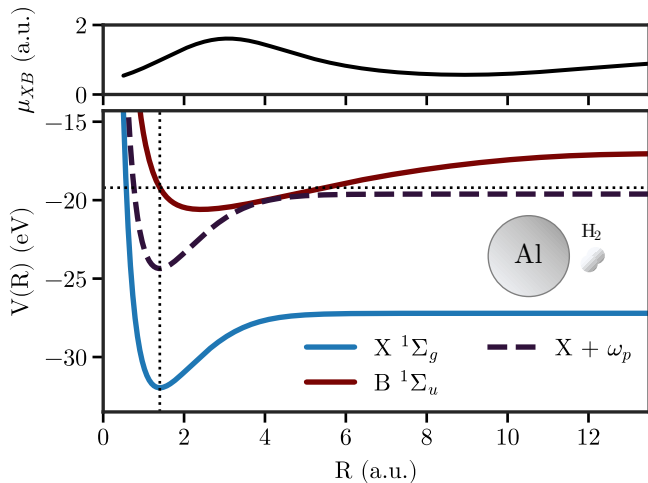


FIG. 1. Main panel: Potential energy curves of the ground (X , light blue) and first excited (B , dark red) states of H_2 as a function of internuclear distance R . Also shown is the potential corresponding to the molecule in the ground state and a photon in the cavity (for $\omega_p = 7.6$ eV). Inset: Sketch of the system we consider: A H_2 molecule next to an aluminum nanosphere. Upper panel: Transition dipole matrix element $\mu_{XB}(R)$ between X and B for light polarized along the molecular axis.

Oppenheimer approximation, the ground state X $^1\Sigma_g^+$ and first excited state B $^1\Sigma_u^+$. In the following, we will refer to these states as simply the X and B states, respectively. Rotational motion is neglected, and the potential energy curves $V_X(R)$ and $V_B(R)$ as a function of the one remaining nuclear coordinate, internuclear distance R , are shown in the main panel of Fig. 1. The transition dipole moment between them is aligned along the molecular axis, and its value along that axis, $\mu_{XB}(R)$, is shown in the upper panel of Fig. 1. The values of $V_X(R)$, $V_B(R)$ and $\mu_{XB}(R)$ are taken from accurate reference calculations^{32–34}. Additionally, both the nuclear position and energy of the Franck-Condon point (corresponding to a vertical transition from X to B at the minimum position in X , $R_{\text{FC}} \approx 1.4$ a.u.) are shown in dashed black lines. As its energy is significantly below the dissociation limit of the B state, $V_B(R \rightarrow \infty)$, photoexcitation will typically not lead to dissociation in the bare molecule (under instantaneous excitation, the dissociation probability is approximately 1%).

The aluminum nanoparticle is modeled as a perfect sphere and represented by a single bosonic mode describing a plasmonic pseudomode^{35–37}. Such a pseudomode corresponds to a highly localized excitation arising as a coherent superposition of many high-order multipole modes with similar frequencies. For sufficiently short distances between the molecule and the nanoparticle (on the order of a few nanometers and below), the pseudomode is by far the most strongly coupled mode. When treated perturbatively (i.e., under the assumption of weak light-matter coupling), it is responsible for quenching^{38–41}, but this simple picture breaks down at short emitter-nanoparticle distances where the coupling becomes comparable to the decay rates and the strong-coupling regime is entered³⁶. Although such pseudomodes are nonradiative and cannot be

excited (and thus detected or characterized) by far-field radiation, they can still be used as effective quantized “cavity” modes with large coupling strengths that can be useful for applications in polaritonic chemistry and molecular polaritonics, such as photoprotection²⁹. In order to quantize the pseudomode we calculate the electromagnetic spectral density⁴² $J(\omega) = \frac{\mu^2 \omega^2}{\pi \hbar \epsilon_0 c^2} \vec{n} \cdot \text{Im} \mathbf{G}(\vec{r}_e, \vec{r}_e, \omega) \cdot \vec{n}$, where $\mathbf{G}(\vec{r}_1, \vec{r}_2, \omega)$ is the dyadic Green’s function solving the (macroscopic) Maxwell equations at frequency ω , \vec{r}_e is the emitter position, \vec{n} is the orientation of its transition dipole moment, and μ is its amplitude. We then use the well-known fact that Lorentzian peaks in $J(\omega)/\mu^2$ correspond to lossy quantized modes with mode energy ω_p , loss rate κ , and single-photon field strength $E_{1\text{ph}}$ determined by the peak position, bandwidth, and amplitude of the peaks^{35,36,43–45}. While this approach can be extended to more complex spectral densities by allowing interactions between the quantized modes⁴⁶, this is not necessary here as the relevant spectral densities are dominated by a single peak.

The Hamiltonian resulting from the above considerations is ($\hbar = 1$ here and in the following)

$$H = \omega_p a^\dagger a + V_X(R) + \omega_m(R) \sigma^\dagger \sigma + E_{1\text{ph}} \mu_{XB}(R) (\sigma^\dagger a + \sigma a^\dagger), \quad (1)$$

where a , a^\dagger are the plasmon annihilation and creation operators, $\omega_m(R) = V_B(R) - V_X(R)$ is the position-dependent molecular excitation energy, and $\sigma = |X\rangle\langle B|$ is the molecular de-excitation operator. We have here treated the light-matter interaction within the dipole approximation, and additionally used the rotating wave approximation in which the total number of excitations (molecular excitations + photons) is conserved. This is a good approximation as long as the coupling strength is small compared to the transition energies, i.e., the system does not enter ultrastrong coupling⁴⁷. We also note that the pseudomode (and nanoparticle plasmons in general) are to a very good approximation quasistatic excitations that only interact with the molecule through the longitudinal electric field (i.e., Coulomb interactions). This has the consequence that irrespective of whether the quantized EM field is treated using minimal coupling or in the Power-Zienau-Woolley picture, the light-matter interaction within the dipole approximation is simply given by $\vec{E} \cdot \vec{\mu}$ and no dipole self-energy term is present in the Hamiltonian^{48,49}.

In the following, we will use the notation $|i, n\rangle$, with $i = (X, B)$ and $n = (0, 1, \dots)$, for the combined electronic-photonic state. The main panel in Fig. 1 additionally shows the potential energy surface for the state $|X, 1\rangle$, corresponding to the molecule in its ground state and a single plasmon excitation. The associated potential energy is simply $V_X(R) + \omega_p$, i.e., the ground-state potential energy surface shifted upwards by that amount^{2,13}. The plasmon energy $\omega_p = 7.6$ eV is chosen such that the curves corresponding to plasmonic and molecular excitation touch tangentially (at $R \approx 4$ a.u.) while the dissociation limit of the $|X, 1\rangle$ curve lies below the Franck-Condon energy for excitation of the bare molecule (the $|B, 0\rangle$ state). This already implies that from purely energetic considerations, the presence of the plasmonic nanoparticle can open a photodissociation channel that does not exist in the bare molecule. In the

following, we will show that this cavity-enabled photodissociation channel indeed is opened and will discuss its properties. Taking into account the ultrafast decay of the plasmonic pseudomode, we have to explicitly treat dissipation in the system in order to obtain an accurate representation of the dynamics of the coupled system. As mentioned above, a mode corresponding to a Lorentzian peak in the spectral density leads to dynamics described by a Lindblad master equation^{50,51} for the system density matrix ρ ,

$$\partial_t \rho = -i[H, \rho] + \kappa L_a[\rho], \quad (2)$$

where $L_A[\rho] = A\rho A^\dagger - \frac{1}{2}\{A^\dagger A, \rho\}$ is a *Lindblad dissipator*, with $\{A, B\} = AB + BA$ the anticommutator. The second term in $L_A[\rho]$ is responsible for probability disappearing from the decaying state, while the first term makes it reappear in the new state that the decay leads to. The first term is thus also variously called the “refilling”, “feeding”, or “quantum jump” term. Eq. (2) can be rewritten as

$$\partial_t \rho = -i(H_{\text{eff}}\rho - \rho H_{\text{eff}}^\dagger) + \kappa \rho a^\dagger \quad (3)$$

where $H_{\text{eff}} = H - \frac{i}{2}\kappa a^\dagger a$ is an effective non-Hermitian Hamiltonian. While we solve the full Lindblad master equation here, we mention that in situations where the refilling term is negligible⁵² or the state reached by it is not of interest²⁹, the dynamics can equivalently be described by the Schrödinger equation of a wave function evolving with the effective Hamiltonian⁵³, leading to significant savings in computational effort as only a wave function instead of a density matrix has to be propagated. However, this simplification is not applicable when the wave packet dynamics after decay are required³¹, as is the case for the setup discussed here.

We numerically discretize the nuclear coordinate R using a finite element discrete variable representation (FEDVR)^{54,55} in which the domain is split into finite elements and a high-order DVR basis is used in each element. This approach allows for high flexibility in adapting both the element size and polynomial order to the local requirements of the problem, while still leading to a very sparse representation of derivative operators and potentials as block-diagonal and diagonal matrices, respectively. It typically achieves significantly higher precision than finite difference grids for the same computational effort. Most calculations shown below use 46 equally sized elements spanning from $R = 0.5$ a.u. to $R = 17$ a.u., with polynomial order 9 inside each element, leading to 369 nuclear basis functions. Some results are obtained with “better” grids, but we have checked that the results are visually indistinguishable from those obtained with the parameters given here, and thus do not mention those cases explicitly. In order to prevent unphysical reflections at the end of the grid when the molecule dissociates, we additionally introduce a complex absorbing potential for $R > R_{\text{abs}}$, given by $V_{\text{abs}}(R) = C(R - R_{\text{abs}})^4$, where $R_{\text{abs}} = 12$ a.u. and $C = 10^{-4}$ a.u. determines the strength of the absorber. In order to maintain trace-preserving dynamics, we introduce this potential through Lindblad dissipators to a fictitious “dissipated” nuclear basis function $|R_{\mathcal{D}}\rangle$ that is not otherwise coupled to the system. The absorbing potential is then described by additional Lindblad dissipators in the master

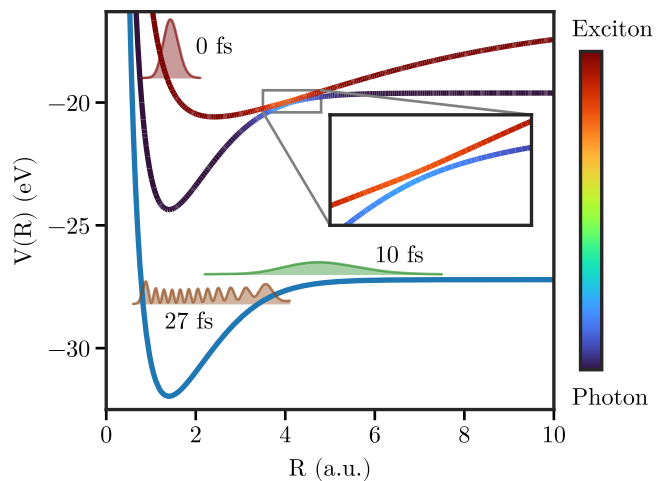


FIG. 2. Polaritonic potential energy curves calculated using the effective non-Hermitian Hamiltonian defined in Eq. (3), for a single-photon field strength of $E_{1\text{ph}} = 70$ mV/ a_0 and cavity loss rate $\kappa = 0.476$ eV. The line color indicates the degree of hybridization. The zoom shows the region where the uncoupled curves become (nearly) degenerate. Also shown are three snapshots of the nuclear wave packet at $t = 0$ fs, $t = 10$ fs, and $t = 27$ fs (the amplitude for the latter two is multiplied by a factor 5 for better visibility). For $t = 27$ fs, a tail corresponding to the dissociating part of the wavepacket at $R > 4$ a.u. is not shown.

equation,

$$\partial_t \rho = -i[H, \rho] + \kappa L_a[\rho] + \sum_{i=1}^{N_i} 2V_{\text{abs}}(R_i)L_{|R_{\mathcal{D}}\rangle\langle R_i|}[\rho], \quad (4)$$

where $|R_i\rangle$ is the FEDVR basis function corresponding to nuclear position R_i . These additional dissipators add a complex absorbing potential to the effective Hamiltonian, while also collecting the absorbed probability in the density matrix at “grid point” $R_{\mathcal{D}}$. This approach allows straightforward monitoring of the electronic-plasmonic potential energy curve on which absorption (i.e., dissociation) happened.

For the numerical implementation, we rely on NumPy⁵⁶ and QuTiP^{57,58}. Since the master equations become relatively large, we have implemented a custom master equation solver that runs on graphics processing units (GPU) by exploiting the CUDA.jl^{59,60} and DifferentialEquations.jl^{61,62} packages for the Julia language⁶³. All plots were prepared using matplotlib^{64,65}.

III. RESULTS

We initially set a plasmon mode frequency of $\omega_p = 7.6$ eV with decay rate $\kappa = 0.476$ eV and quantized field strength $E_{1\text{ph}} = 70$ mV/ a_0 , where a_0 is the Bohr radius⁶⁶. These parameters correspond approximately to a hydrogen molecule at a distance of slightly less than 1 nm from an aluminum nanosphere with a radius of 20 nm embedded in a background dielectric material with refractive index $n = 1.75$. The corresponding polaritonic potential energy curves², calculated using the effective Hamiltonian, are shown in Fig. 2. The dynamics

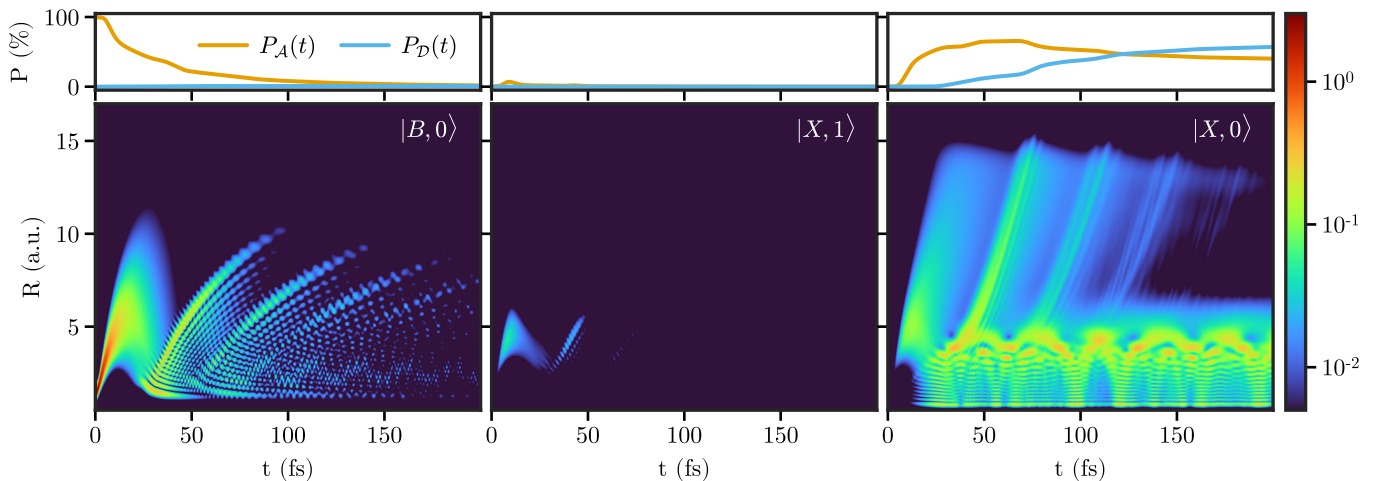


FIG. 3. Lower panels: Nuclear wavepacket (probability density) corresponding to the excited molecule, $|B, 0\rangle$, a plasmon excitation in the nanoparticle $|X, 1\rangle$, and the ground state $|X, 0\rangle$ as a function of time. Upper panels: Total integrated probability $P_{\mathcal{A}}(t)$ in the “active” nuclear region and probability $P_{\mathcal{D}}(t)$ of dissociation for each electronic-plasmonic state.

are initialized assuming ultrafast vertical excitation from X to B , i.e., with an initial state that corresponds to the vibrational ground state on $V_X(R)$ promoted to $V_B(R)$. This initial wavepacket is shown in Fig. 2 in red. The vertical excitation energy at the equilibrium position $R_0 \approx 1.4$ a.u. corresponds to $\omega_m(R_0) \approx 12.75$ eV, far detuned from the plasmon resonance. As the wavepacket starts oscillating and spreading on the B curve, within less than 10 fs it reaches the region where the cavity and molecular transition are on resonance. There, the coupling to the plasmonic mode leads to population transfer into the plasmonically excited surface, which almost immediately decays to the ground state. As we have recently shown, the photons emitted from a plasmonic cavity in similar setups can give direct optical access to ultrafast nuclear motion²⁷. However, in the current case, the plasmonic mode is nonradiative and no photons are emitted into the far field. Nonetheless, the plasmonic decay conserves the kinetic energy accumulated by the nuclear wavepacket during its propagation on the B surface⁶⁷. The nuclear wavepacket arriving on the ground-state surface $V_X(R)$ (shown in green at $t = 10$ fs in Fig. 2) can thus keep propagating, with a significant fraction overcoming the dissociation barrier. At the same time, some fraction of the wavepacket remains trapped in the bound vibrational states of $V_X(R)$, shown in brown for $t = 27$ fs in Fig. 2.

To get detailed insight into the wavepacket dynamics, we show the nuclear probability density on each of the three relevant states $|B, 0\rangle$, $|X, 1\rangle$, and $|X, 0\rangle$ as a function of time in Fig. 3. This shows the nuclear wavepacket initially oscillating on the molecular excited state $|B, 0\rangle$. The light-matter coupling then leads to efficient energy transfer to the plasmonic state $|X, 1\rangle$ at the nuclear positions where they are close in energy, roughly between $R = 3$ a.u. and $R = 7$ a.u. The plasmonic state almost immediately decays after excitation, such that the wavepacket is directly transferred to the $|X, 0\rangle$ state. However, it is clearly visible in the third panel of Fig. 3 that a significant fraction of the wavepacket that decays to the ground state overcomes the dissociation barrier and propagates to large in-

ternuclear distances R , where it is absorbed by the absorbing potential. Since the nuclear wavepacket in the lower panels of Fig. 3 is shown in logarithmic scale, which inhibits easy visual interpretation of absolute probabilities, in the upper panels we additionally show the integrated probabilities in the “active” nuclear region of each electronic-plasmonic state, $P_{\mathcal{A}}(t)$, as well as the already dissociated component $P_{\mathcal{D}}(t)$. This demonstrates clearly that the light-matter coupling through the plasmonic pseudomode induces ultrafast decay of the nuclear wavepacket from the initial excited state, with most of the probability disappearing within about 100 fs. Furthermore, it also shows that after decaying to the ground state $|X, 0\rangle$, a significant portion of the nuclear wavepacket dissociates, reaching more than 50% for the present parameters. The remaining wavepacket ends up in bound vibrational levels on the ground-state surface.

We note that due to the highly lossy nature of aluminum, the decay rate of the pseudomode (and other plasmonic resonances) is quite large ($\kappa = 0.476$ eV), with an associated lifetime of only $\tau = \hbar/\kappa \approx 1.38$ fs, even shorter than for the more commonly used metals such as gold or silver, which have plasmon resonances in the visible spectrum. The strong coupling regime is entered when $g > \kappa/4$ if the condition is taken that at resonance $\omega_p = \omega_m(R)$, the real part of the eigenenergies of the effective Hamiltonian starts to split, and for slightly larger g if one requires that the corresponding peaks can be spectrally distinguished⁶⁸. The maximum value of the transition dipole moment $\mu_{XB}(R)$ is approximately $1.61 e a_0$, reached at $R = 3.1$ a.u. For realistic parameters, with $E_{1\text{ph}}$ reaching up to about $100 \text{ mV}/a_0$, the system we treat will thus stay within the weak coupling regime or at best barely enter strong coupling. However, since the coupling is quite strong even when smaller than the decay rate, the plasmonic pseudomode serves as an effective decay channel at internuclear distances where $\omega_m(R)$ is sufficiently close to ω_p . The ultrafast decay we see above can thus be understood to a good approximation as an extreme Purcell effect, with the emissive lifetime decreasing from about ≈ 0.5 ns for the bare molecule down to the femtosecond scale

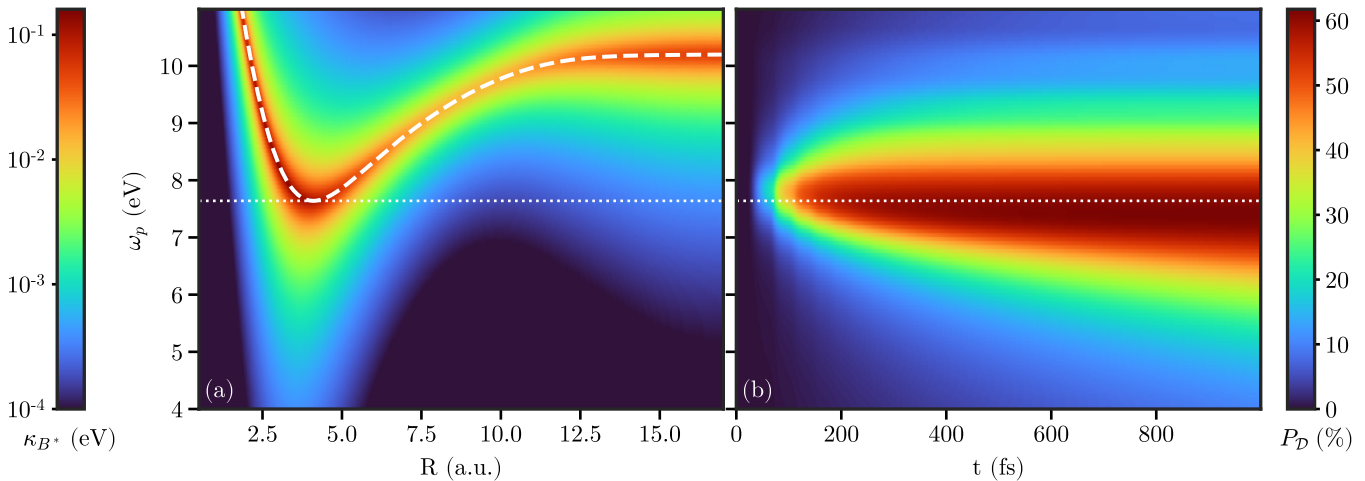


FIG. 4. (a): Coupling-induced decay rate $\kappa_{B^*}(R)$ on the polaritonic potential energy curve corresponding to the molecular excited state as a function of plasmon mode frequency ω_p . The dashed white line corresponds to the molecular excitation frequency $\omega_m(R)$. (b): Dissociation probability after 1000 fs for the same conditions. The dotted white line in both panels marks the minimum value of $\omega_m(R)$.

due to the pseudomode. However, it should be stressed that an important aspect of the strategy we propose is the energy selectivity of the plasmonic pseudomode, i.e., the fact that it does not “just” enhance emission, but does so at a specific energy. Within a temporal picture, this allows to enhance decay at nuclear positions where the initial wavepacket has already accumulated enough kinetic energy to subsequently dissociate. Energetically, the approach can be understood as selecting the energy difference between the initially absorbed photon and the subsequently emitted one. This difference is necessarily converted into vibrational energy (like in Raman scattering) which can then be used to dissociate the molecule in its ground state. A further important point is that this process happens on ultrafast timescales, so that, e.g., intramolecular vibrational energy redistribution (which would only occur in more complex molecules with multiple nuclear degrees of freedom) does not have time to dissipate the accumulated kinetic energy between different modes.

We thus next explore the energy sensitivity of the loss-induced photodissociation process in more detail. To do so, we scan the frequency of the plasmonic pseudomode ω_p over a large interval (from 4 to 11 eV) while keeping all other parameters fixed. Since for the given coupling strength, the system is mostly in the weak coupling regime, a useful quantity to plot is the induced effective decay rate of the (cavity-modified) excited molecular state B^* . Here, the asterisk denotes polaritonic states obtained by diagonalizing the effective Hamiltonian H_{eff} within the Born-Oppenheimer approximation (i.e., separately for each R), and B^* is the state that is closest in character to the bare molecular excited state B . In the effective Hamiltonian, the energies (and thus the polaritonic PES) become complex, and the local decay rates are given by $\kappa_{B^*}(R) = -2\text{Im}V_{B^*}(R)$. Within the (almost) weak coupling regime considered here, the modifications of the real part of the surface are much smaller, $\text{Re}V_{B^*}(R) \approx V_B(R)$. We thus show $\kappa_{B^*}(R)$ as a function of plasmon frequency ω_p in Fig. 4(a). The white dashed line in the figure is given by $\omega_m(R)$,

i.e., the position-dependent molecular excitation energy. The plasmon-induced molecular decay rate is most strongly enhanced when the plasmon is on resonance with the molecular transition, $\omega_p \approx \omega_m(R)$, as could be expected and has been previously proposed as a tool for probing molecular dynamics by ultrafast emission²⁷. The cavity-induced decay rate for non-zero detuning depends on both the detuning and the coupling strength. For $g(R) = E_{\text{1ph}}\mu_{XB}(R) \ll \kappa/4$, it can be well approximated by a Lorentzian function, $\kappa_{B^*}(R) \approx \frac{4g(R)^2}{4\delta(R)^2 + \kappa^2}$, where $\delta(R) = \omega_m(R) - \omega_p$.

We now focus on how this frequency dependence of the pseudomode-induced decay affects the photodissociation process. To that end, Fig. 4(b) shows the total dissociation probability as a function of time for the same range of plasmon frequencies. We first note that at short times, there is a step-wise behavior that stems from the initially localized character of the nuclear wavepacket, which creates a burst of dissociation every time it passes the nuclear distances where decay is efficient²⁷, and then proceeds towards dissociation. At later times, the nuclear wavepacket delocalizes due to the non-harmonic character of the involved potentials, and the step-wise behavior is washed out.

As a function of frequency, there is a dominant peak centered just below $\omega_p = \min \omega_m(R)$, i.e., the minimum of the molecular transition frequency (indicated by a thin dotted white line in the figure). This reinforces that, as discussed above, the molecular decay rate shown in panel (a) does not by itself determine the dissociation probability. In addition to inducing ultrafast decay on the excited-state surface, the decay has to happen after the wavepacket acquires enough vibrational energy to dissociate after reaching the ground state. This consideration implies that smaller ω_p should be favored, as less of the total available energy is then spent on creating the plasmon excitation, and the remainder can be used for overcoming the dissociation barrier. Combining this with the competing requirement of being close to resonance to achieve efficient decay explains

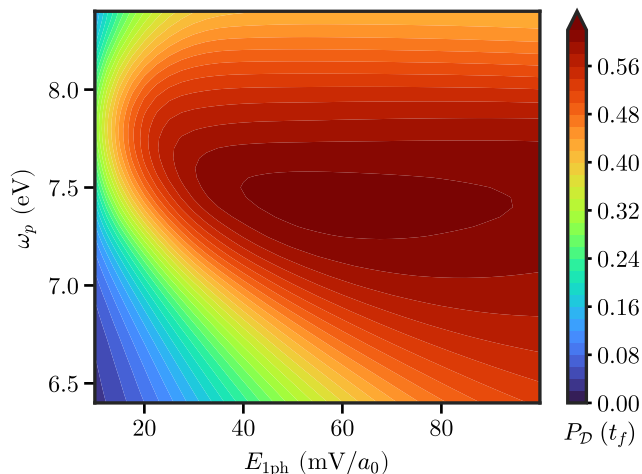


FIG. 5. Dissociation probability $P_{\mathcal{D}}(t_f)$ at $t_f = 1000$ fs as a function of single-photon field strength $E_{1\text{ph}}$ and plasmon mode frequency ω_p .

the results observed here. However, it should additionally be noted that while at the maximum times considered here, both very low and very high plasmon frequencies appear similarly efficient in inducing dissociation, their long-time behavior is markedly different: While at high frequencies, the wavepacket decays efficiently (at least as long as the cavity frequency is not significantly above the molecular excitation frequency at the Franck-Condon point, $\omega_m(R_{\text{FC}}) \approx 12.75$ eV, higher than the frequencies considered here), it primarily does so with little vibrational energy and thus stays in the bound vibrational states on the electronic ground state curve $V_X(R)$. In contrast, the induced decay slows down when the plasmon frequency is below the minimum of $\omega_m(R)$, but the wave packet after decay acquires considerable vibrational energy and can thus dissociate with high probability. The end result is that at high frequencies, the dissociation probability is already essentially saturated for the latest time shown in Fig. 4(b), $t_f = 1000$ fs, while at low frequencies it keeps rising even at longer times. For the lowest frequency considered, $\omega_p = 4$ eV, the dissociation probability rises to over 45% when propagation is performed until $t = 10$ ps, and fitting to an exponential saturation curve implies that the limiting value is $P_{\mathcal{D}}(t \rightarrow \infty) \approx 49\%$. This implies that the plasmon-induced photodissociation efficiency at lower plasmon frequencies can also be significant, but the reduced speed means that this case is more sensitive to effects not considered here (such as collisions or intramolecular vibrational energy redistribution in more complex molecules).

We finally check how strongly the effects studied here depend on the coupling strength to the plasmon mode, which is strongly dependent on the distance to the nanoparticle. The total dissociation probability at time $t_f = 1000$ fs is shown as a function of plasmon frequency ω_p and quantized single-photon field strength $E_{1\text{ph}}$ in Fig. 5. The considered values for $E_{1\text{ph}}$, ranging from $10 \text{ mV}/a_0$ to $100 \text{ mV}/a_0$, correspond to distances of roughly 0.5 nm to 2 nm , which lies within the experimentally accessible range for nanoplasmonic antennas^{24,25}. The effective mode volume, $V_{\text{eff}} = \hbar\omega_p / (2\epsilon_0 E_{1\text{ph}}^2)$ for the largest

couplings considered here is on the order of 20 nm^3 . While we stay within a single-mode description here, it should be noted that for increasing distances, the pseudomode stops being the most strongly coupled mode, and the dipole mode (which is radiative and has lower frequency) becomes dominant³⁶. Fig. 5 shows that, as could be expected, increasing coupling strengths lead to increasing dissociation efficiency. It can also be appreciated that the frequency range over which dissociation is efficient increases with increasing field confinement (i.e., larger $E_{1\text{ph}}$). However, we also find that there is an optimal value for the coupling strength, i.e., the photodissociation probability starts dropping again as the coupling strength increases above an optimal value. Consistent with results found in the photoprotection efficiency of uracil molecules²⁹, the optimal value is close to the onset of the strong-coupling regime. While the situation in a molecule with nuclear motion is somewhat more complicated than in two-level emitters, the underlying reason for this can be understood by taking into account that plasmon-induced decay is most efficient just at the limit between weak and strong coupling⁶⁹, where the effective Hamiltonian has an exceptional point⁷⁰.

IV. SUMMARY

To summarize, we have theoretically investigated a strategy for using highly lossy plasmonic modes to enable and enhance photodissociation in molecules for which the excited-state surface reached by photoexcitation is non-dissociative. We used the H_2 molecule next to an aluminum nanoparticle as a model system. For short distances, the extremely localized and non-radiative plasmonic pseudomode then functions as an effective “cavity” mode with extreme sub-wavelength field confinement. The basic idea of the strategy we proposed is to use a resonantly enhanced Raman-like process where part of the energy absorbed from an exciting photon is resonantly emitted into a lower-energy plasmon resonance, with the remaining energy converted to vibrational excitation on the molecular ground state. If this energy is high enough, the nuclear wavepacket can then overcome the dissociation barrier. Making use of the unavoidable high losses of plasmonic nanoantenna modes, the induced ultrafast decay rates ensure that the whole process takes place on femtosecond scales, faster than other relevant processes leading to energy dissipation.

We have studied in detail how the process depends on the properties of the plasmonic modes, in particular their frequency and the achieved field confinement, and have found that there are competing effects leading to a pronounced maximum as a function of cavity frequency: On the one hand, lower plasmon frequencies leave more of the initial energy available as vibrational energy for the wavepacket after decay, while on the other hand, resonance between the plasmon and molecular excitation enhances the overall decay rate on the plasmon-modified potential energy curve. The competition between these two effects leads to a maximum of dissociation efficiency close to the minimum excitation energy of the molecule, i.e., at the point where the ground- and excited-state surfaces are closest to each other.

The strategy we have presented adds to the growing repertoire of loss-induced phenomena in molecular polaritonic and polaritonic chemistry^{27–31}. This field has enjoyed increasing interest recently as a way to make virtue out of necessity in nanoplasmonic systems, where extreme subwavelength confinement can provide coupling strengths close to or within the single-molecule strong-coupling regime at room temperature, but losses on the femtosecond scale are unavoidable.

ACKNOWLEDGMENTS

We thank Alicia Palacios for insightful discussions and for providing the PES of the hydrogen molecule in digitalized form. This work has been funded by the European Research Council through grant ERC-2016-StG-714870, and by the Spanish Ministry for Science, Innovation, and Universities – Agencia Estatal de Investigación through grants RTI2018-099737-B-I00, PCI2018-093145 (through the QuantERA program of the European Commission), and CEX2018-000805-M (through the María de Maeztu program for Units of Excellence in R&D).

DATA AVAILABILITY STATEMENT

The data that support the findings of this study are available from the corresponding author upon reasonable request.

- ¹T. W. Ebbesen, “Hybrid Light–Matter States in a Molecular and Material Science Perspective,” *Acc. Chem. Res.* **49**, 2403 (2016).
- ²J. Feist, J. Galego, and F. J. Garcia-Vidal, “Polaritonic Chemistry with Organic Molecules,” *ACS Photonics* **5**, 205 (2018).
- ³M. Ruggenthaler, N. Tancogne-Dejean, J. Flick, H. Appel, and A. Rubio, “From a Quantum-Electrodynamical Light–Matter Description to Novel Spectroscopies,” *Nat. Rev. Chem.* **2**, 0118 (2018).
- ⁴R. F. Ribeiro, L. A. Martínez-Martínez, M. Du, J. Campos-Gonzalez-Angulo, and J. Yuen-Zhou, “Polariton Chemistry: Controlling Molecular Dynamics with Optical Cavities,” *Chem. Sci.* **9**, 6325 (2018).
- ⁵M. Hertzog, M. Wang, J. Mony, and K. Börjesson, “Strong Light–Matter Interactions: A New Direction within Chemistry,” *Chem. Soc. Rev.* **48**, 937 (2019).
- ⁶F. Herrera and J. Owrutsky, “Molecular Polaritons for Controlling Chemistry with Quantum Optics,” *J. Chem. Phys.* **152**, 100902 (2020).
- ⁷D. G. Lidzey, D. D. C. Bradley, T. Virgili, A. Armitage, M. S. Skolnick, and S. Walker, “Room Temperature Polariton Emission from Strongly Coupled Organic Semiconductor Microcavities,” *Phys. Rev. Lett.* **82**, 3316 (1999).
- ⁸T. Schwartz, J. A. Hutchison, C. Genet, and T. W. Ebbesen, “Reversible Switching of Ultrastrong Light-Molecule Coupling,” *Phys. Rev. Lett.* **106**, 196405 (2011).
- ⁹J. A. Hutchison, T. Schwartz, C. Genet, E. Devaux, and T. W. Ebbesen, “Modifying Chemical Landscapes by Coupling to Vacuum Fields,” *Angew. Chem.* **124**, 1624 (2012).
- ¹⁰K. Stranius, M. Hertzog, and K. Börjesson, “Selective Manipulation of Electronically Excited States through Strong Light–Matter Interactions,” *Nat. Commun.* **9**, 2273 (2018).
- ¹¹V. N. Peters, M. O. Faruk, J. Asane, R. Alexander, D. A. Peters, S. Prayakara, S. Rout, and M. A. Noginov, “Effect of Strong Coupling on Photodegradation of the Semiconducting Polymer P3HT,” *Optica* **6**, 318 (2019).
- ¹²D. Polak, R. Jayaprakash, T. P. Lyons, L. Á. Martínez-Martínez, A. Leventis, K. J. Fallon, H. Coulthard, D. G. Bossanyi, K. Georgiou, I. I. Anthony J. Petty, J. Anthony, H. Bronstein, J. Yuen-Zhou, A. I. Tartakovskii, J. Clark, and A. J. Musser, “Manipulating Molecules with Strong Coupling: Harvesting Triplet Excitons in Organic Exciton Microcavities,” *Chem. Sci.* **11**, 343 (2020).
- ¹³J. Galego, F. J. Garcia-Vidal, and J. Feist, “Cavity-Induced Modifications of Molecular Structure in the Strong-Coupling Regime,” *Phys. Rev. X* **5**, 041022 (2015).
- ¹⁴F. Herrera and F. C. Spano, “Cavity-Controlled Chemistry in Molecular Ensembles,” *Phys. Rev. Lett.* **116**, 238301 (2016).
- ¹⁵M. Kowalewski, K. Bennett, and S. Mukamel, “Cavity Femtochemistry: Manipulating Nonadiabatic Dynamics at Avoided Crossings,” *J. Phys. Chem. Lett.* **7**, 2050 (2016).
- ¹⁶J. Galego, F. J. Garcia-Vidal, and J. Feist, “Suppressing Photochemical Reactions with Quantized Light Fields,” *Nat. Commun.* **7**, 13841 (2016).
- ¹⁷J. Galego, F. J. Garcia-Vidal, and J. Feist, “Many-Molecule Reaction Triggered by a Single Photon in Polaritonic Chemistry,” *Phys. Rev. Lett.* **119**, 136001 (2017).
- ¹⁸O. Vendrell, “Collective Jahn-Teller Interactions through Light-Matter Coupling in a Cavity,” *Phys. Rev. Lett.* **121**, 253001 (2018).
- ¹⁹G. Groenhof and J. J. Toppari, “Coherent Light Harvesting through Strong Coupling to Confined Light,” *J. Phys. Chem. Lett.* **9**, 4848 (2018).
- ²⁰G. Groenhof, C. Climent, J. Feist, D. Morozov, and J. J. Toppari, “Tracking Polariton Relaxation with Multiscale Molecular Dynamics Simulations,” *J. Phys. Chem. Lett.* **10**, 5476 (2019).
- ²¹J. A. Ćwik, P. Kirton, S. De Liberato, and J. Keeling, “Excitonic Spectral Features in Strongly Coupled Organic Polaritons,” *Phys. Rev. A* **93**, 033840 (2016).
- ²²J. B. Khurgin, “How to Deal with the Loss in Plasmonics and Metamaterials,” *Nat. Nanotechnol.* **10**, 2 (2015).
- ²³G. Zengin, M. Wersäll, S. Nilsson, T. J. Antosiewicz, M. Käll, and T. Shegai, “Realizing Strong Light-Matter Interactions between Single-Nanoparticle Plasmons and Molecular Excitons at Ambient Conditions,” *Phys. Rev. Lett.* **114**, 157401 (2015).
- ²⁴R. Chikkaraddy, B. de Nijs, F. Benz, S. J. Barrow, O. A. Scherman, E. Rosta, A. Demetriadou, P. Fox, O. Hess, and J. J. Baumberg, “Single-Molecule Strong Coupling at Room Temperature in Plasmonic Nanocavities,” *Nature* **535**, 127 (2016).
- ²⁵O. S. Ojambati, R. Chikkaraddy, W. D. Deacon, M. Horton, D. Kos, V. A. Turek, U. F. Keyser, and J. J. Baumberg, “Quantum Electrodynamics at Room Temperature Coupling a Single Vibrating Molecule with a Plasmonic Nanocavity,” *Nat. Commun.* **10**, 1049 (2019).
- ²⁶B. Munkhbat, M. Wersäll, D. G. Baranov, T. J. Antosiewicz, and T. Shegai, “Suppression of Photo-Oxidation of Organic Chromophores by Strong Coupling to Plasmonic Nanoantennas,” *Sci. Adv.* **4**, eaas9552 (2018).
- ²⁷R. E. F. Silva, J. del Pino, F. J. Garcia-Vidal, and J. Feist, “Polaritonic Molecular Clock for All-Optical Ultrafast Imaging of Wavepacket Dynamics without Probe Pulses,” *Nat. Commun.* **11**, 1423 (2020).
- ²⁸I. S. Ulusoy and O. Vendrell, “Dynamics and Spectroscopy of Molecular Ensembles in a Lossy Microcavity,” *J. Chem. Phys.* **153**, 044108 (2020).
- ²⁹S. Felicetti, J. Fregoni, T. Schnappinger, S. Reiter, R. de Vivie-Riedle, and J. Feist, “Photoprotecting Uracil by Coupling with Lossy Nanocavities,” *J. Phys. Chem. Lett.* **11**, 8810 (2020).
- ³⁰P. Antoniou, F. Suchanek, J. F. Varner, and J. J. Foley, “Role of Cavity Losses on Nonadiabatic Couplings and Dynamics in Polaritonic Chemistry,” *J. Phys. Chem. Lett.* **11**, 9063 (2020).
- ³¹E. Davidsson and M. Kowalewski, “Simulating Photodissociation Reactions in Bad Cavities with the Lindblad Equation,” [arXiv:2010.09587](https://arxiv.org/abs/2010.09587).
- ³²L. Wolniewicz, “Relativistic Energies of the Ground State of the Hydrogen Molecule,” *J. Chem. Phys.* **99**, 1851 (1993).
- ³³G. Staszewska and L. Wolniewicz, “Adiabatic Energies of Excited 1Σ States of the Hydrogen Molecule,” *Journal of Molecular Spectroscopy* **212**, 208 (2002).
- ³⁴L. Wolniewicz and G. Staszewska, “ $1\Sigma_g^+ \rightarrow X^1\Sigma_g^+$ Transition Moments for the Hydrogen Molecule,” *Journal of Molecular Spectroscopy* **217**, 181 (2003).
- ³⁵A. González-Tudela, P. A. Huidobro, L. Martín-Moreno, C. Tejedor, and F. J. García-Vidal, “Reversible Dynamics of Single Quantum Emitters near Metal-Dielectric Interfaces,” *Phys. Rev. B* **89**, 041402(R) (2014).
- ³⁶A. Delga, J. Feist, J. Bravo-Abad, and F. J. Garcia-Vidal, “Quantum Emitters Near a Metal Nanoparticle: Strong Coupling and Quenching,” *Phys. Rev. Lett.* **112**, 253601 (2014).
- ³⁷A. Delga, J. Feist, J. Bravo-Abad, and F. J. Garcia-Vidal, “Theory of Strong Coupling between Quantum Emitters and Localized Surface Plasmons,” *J. Opt.* **16**, 114018 (2014).

- ³⁸E. Dulkeith, A. C. Morteani, T. Niedereichholz, T. A. Klar, J. Feldmann, S. A. Levi, F. C. J. M. van Veggel, D. N. Reinhoudt, M. Möller, and D. I. Gittins, "Fluorescence Quenching of Dye Molecules near Gold Nanoparticles: Radiative and Nonradiative Effects," *Phys. Rev. Lett.* **89**, 203002 (2002).
- ³⁹P. Anger, P. Bharadwaj, and L. Novotny, "Enhancement and Quenching of Single-Molecule Fluorescence," *Phys. Rev. Lett.* **96**, 113002 (2006).
- ⁴⁰S. Kühn, U. Håkanson, L. Rogobete, and V. Sandoghdar, "Enhancement of Single-Molecule Fluorescence Using a Gold Nanoparticle as an Optical Nanoantenna," *Phys. Rev. Lett.* **97**, 017402 (2006).
- ⁴¹C. M. Galloway, P. G. Etchegoin, and E. C. Le Ru, "Ultrafast Nonradiative Decay Rates on Metallic Surfaces by Comparing Surface-Enhanced Raman and Fluorescence Signals of Single Molecules," *Phys. Rev. Lett.* **103**, 063003 (2009).
- ⁴²L. Novotny and B. Hecht, *Principles of Nano-Optics*, 2nd ed. (Cambridge University Press, Cambridge, 2012).
- ⁴³A. Imamoglu, "Stochastic Wave-Function Approach to Non-Markovian Systems," *Phys. Rev. A* **50**, 3650 (1994).
- ⁴⁴G. Grynberg, A. Aspect, C. Fabre, and C. Cohen-Tannoudji, *Introduction to Quantum Optics: From the Semi-Classical Approach to Quantized Light* (Cambridge University Press, Cambridge, 2010).
- ⁴⁵B. Rousseaux, D. Dzsofjan, G. Colas des Francs, H. R. Jauslin, C. Couteau, and S. Guérin, "Adiabatic Passage Mediated by Plasmons: A Route towards a Decoherence-Free Quantum Plasmonic Platform," *Phys. Rev. B* **93**, 045422 (2016).
- ⁴⁶I. Medina, F. J. García-Vidal, A. I. Fernández-Domínguez, and J. Feist, "Few-Mode Field Quantization of Arbitrary Electromagnetic Spectral Densities," [arXiv:2008.00349](https://arxiv.org/abs/2008.00349).
- ⁴⁷A. Frisk Kockum, A. Miranowicz, S. D. Liberato, S. Savasta, and F. Nori, "Ultrastrong Coupling between Light and Matter," *Nat. Rev. Phys.* **1**, 19 (2019).
- ⁴⁸J. Galego, C. Climent, F. J. Garcia-Vidal, and J. Feist, "Cavity Casimir-Polder Forces and Their Effects in Ground-State Chemical Reactivity," *Phys. Rev. X* **9**, 021057 (2019).
- ⁴⁹J. Feist, A. I. Fernández-Domínguez, and F. J. García-Vidal, "Macroscopic QED for Quantum Nanophotonics: Emitter-Centered Modes as a Minimal Basis for Multiemitter Problems," *Nanophotonics*, (advance online publication) (2020).
- ⁵⁰G. Lindblad, "On the Generators of Quantum Dynamical Semigroups," *Commun. Math. Phys.* **48**, 119 (1976).
- ⁵¹D. Manzano, "A Short Introduction to the Lindblad Master Equation," *AIP Advances* **10**, 025106 (2020).
- ⁵²R. Sáez-Blázquez, J. Feist, A. I. Fernández-Domínguez, and F. J. García-Vidal, "Enhancing Photon Correlations through Plasmonic Strong Coupling," *Optica* **4**, 1363 (2017).
- ⁵³P. M. Visser and G. Nienhuis, "Solution of Quantum Master Equations in Terms of a Non-Hermitian Hamiltonian," *Phys. Rev. A* **52**, 4727 (1995).
- ⁵⁴T. N. Rescigno and C. W. McCurdy, "Numerical Grid Methods for Quantum-Mechanical Scattering Problems," *Phys. Rev. A* **62**, 32706 (2000).
- ⁵⁵B. I. Schneider and L. A. Collins, "The Discrete Variable Method for the Solution of the Time-Dependent Schrödinger Equation," *J. Non-Cryst. Solids* **351**, 1551 (2005).
- ⁵⁶C. R. Harris, K. J. Millman, S. J. van der Walt, R. Gommers, P. Virtanen, D. Cournapeau, E. Wieser, J. Taylor, S. Berg, N. J. Smith, R. Kern, M. Picus, S. Hoyer, M. H. van Kerkwijk, M. Brett, A. Haldane, J. F. del Río, M. Wiebe, P. Peterson, P. Gérard-Marchant, K. Sheppard, T. Reddy, W. Weckesser, H. Abbasi, C. Gohlke, and T. E. Oliphant, "Array Programming with NumPy," *Nature* **585**, 357 (2020).
- ⁵⁷J. R. Johansson, P. D. Nation, and F. Nori, "QuTiP: An Open-Source Python Framework for the Dynamics of Open Quantum Systems," *Comput. Phys. Commun.* **183**, 1760 (2012).
- ⁵⁸J. R. Johansson, P. D. Nation, and F. Nori, "QuTiP 2: A Python Framework for the Dynamics of Open Quantum Systems," *Comput. Phys. Commun.* **184**, 1234 (2013).
- ⁵⁹T. Besard, C. Foket, and B. D. Sutter, "Effective Extensible Programming: Unleashing Julia on GPUs," *IEEE Trans. Parallel Distrib. Syst.* **30**, 827 (2019).
- ⁶⁰T. Besard, V. Churavy, A. Edelman, and B. D. Sutter, "Rapid Software Prototyping for Heterogeneous and Distributed Platforms," *Advances in Engineering Software* **132**, 29 (2019).
- ⁶¹C. Rackauckas and Q. Nie, "DifferentialEquations.jl – A Performant and Feature-Rich Ecosystem for Solving Differential Equations in Julia," *J. Open Res. Softw.* **5**, 15 (2017).
- ⁶²C. Rackauckas and Q. Nie, "Confederated Modular Differential Equation APIs for Accelerated Algorithm Development and Benchmarking," *Advances in Engineering Software* **132**, 1 (2019).
- ⁶³J. Bezanson, A. Edelman, S. Karpinski, and V. B. Shah, "Julia: A Fresh Approach to Numerical Computing," *SIAM Rev.* **59**, 65 (2017).
- ⁶⁴J. D. Hunter, "Matplotlib: A 2D Graphics Environment," *Comput. Sci. Eng.* **9**, 90 (2007).
- ⁶⁵T. A. Caswell, M. Droettboom, A. Lee, J. Hunter, E. Firing, D. Stansby, J. Klymak, T. Hoffmann, E. Sales de Andrade, N. Varoquaux, J. Hedegaard Nielsen, B. Root, P. Elson, R. May, D. Dale, J.-J. Lee, J. K. Seppänen, D. McDougall, A. Straw, P. Hobson, C. Gohlke, T. S. Yu, E. Ma, A. F. Vincent, S. Silvester, C. Moad, N. Kniazev, P. Ivanov, E. Ernest, and J. Katins, "Matplotlib v3.2.1," Zenodo (2020).
- ⁶⁶These uncommon units for the electric field strength, $1 \text{ mV}/a_0 \approx 18.9 \text{ MV}/\text{m}$, allow straightforward calculation of the light-matter coupling strength $g = E_{1\text{ph}}\mu$ in meV for a transition dipole μ given in atomic units ea_0 , as in Fig. 1.
- ⁶⁷A. Palacios, J. Feist, A. González-Castrillo, J. L. Sanz-Vicario, and F. Martín, "Autoionization of Molecular Hydrogen: Where Do the Fano Lineshapes Go?" *ChemPhysChem* **14**, 1456 (2013).
- ⁶⁸P. Törmä and W. L. Barnes, "Strong Coupling between Surface Plasmon Polaritons and Emitters: A Review," *Rep. Prog. Phys.* **78**, 013901 (2015).
- ⁶⁹S. I. Bozhevolnyi and J. B. Khurgin, "Fundamental Limitations in Spontaneous Emission Rate of Single-Photon Sources," *Optica* **3**, 1418 (2016).
- ⁷⁰R. El-Ganainy, K. G. Makris, M. Khajavikhan, Z. H. Musslimani, S. Rotter, and D. N. Christodoulides, "Non-Hermitian Physics and PT Symmetry," *Nat. Phys.* **14**, 11 (2018).